

The Effects of Supersaturation on the Nucleation of Precipitates in Nickel-Based Superalloys

Undergraduate Researcher
Brent Carey, Clarkson University

Faculty Mentor
David Seidman
Department of Materials Science and Engineering,
Northwestern University

Postdoctoral Mentor
Kevin Yoon
Department of Materials Science and Engineering,
Northwestern University

Abstract

The purpose of this study was to select an alloy with a low driving force for nucleation for a more in-depth study of the nucleation of γ' -precipitates. To do this, three Ni-Cr-Al alloys were chosen close to the solvus line of a Ni-Cr-Al phase diagram, ensuring low supersaturation and therefore a low driving force for precipitate growth. The three alloys chosen — 03-14, 03-15, and 03-16 (Ni-9.0 Cr-7.0 Al atomic percent (at.%), Ni-9.25 Cr-6.75 Al at.%, and Ni-9.5 Cr-6.5 Al at.%, respectively) — were aged at 600° C for 0.25 hours in order to observe forming precipitate nuclei in both the γ -matrix and γ' -precipitates. Three-dimensional atom probe (3DAP) microscopy was performed on these alloys to produce three-dimensional reconstructions of their atomic arrangement to determine the nanostructure and the chemical composition of both the γ and γ' phases. The results for volume fraction, number density, and mean radius of the precipitates, as well as the concentrations of both the matrix and the precipitate phases, were then determined for the 03-15 and 03-16 alloys by analyzing the 3DAP microscopy data. These attributes were previously established for alloy 03-14 in unpublished results by T. Ziebell and K. Yoon. From these results, all three of these alloys were observed to have a lower driving force for

nucleation than the previously studied Ni-14.8 Cr-5.2 Al at.% alloy.¹ Of those three, 03-16 had the lowest Al supersaturation, thereby also having the lowest driving force for nucleation. Given this, alloy 03-16 will be used for a more direct study of the nucleation of precipitates. Transmission electron microscopy (TEM) was also used to confirm the structure of the precipitates. The resultant diffraction pattern was conclusive in showing that the precipitates observed in the three-dimensional reconstructions were in fact $L1_2$ ordered Ni_3Al γ' -precipitates, due to the appearance of superlattice reflections. The presence of γ' -precipitates in these superalloys is important, as $L1_2$ ordered precipitates help to strengthen the alloy by impeding the motion of dislocations through the γ -matrix.

Introduction

The term “superalloy” was coined to characterize alloys that are based on nickel, cobalt, or iron and perform well at elevated temperatures (above 540° C).² The most prominent use of nickel-based superalloys is in the production of both land-based gas turbines and aviation jet engines, as well as in catalytic reactors, nuclear reactors, submarines, petrochemical equipment, and other high-temperature applications.² Of particular technological importance as a result of their dual-phase nanostructure are Ni-Cr-Al superalloys. On a nanoscale level, $L1_2$ ordered Ni_3Al precipitates (γ') are present in a Cr-rich FCC matrix (γ). Due to this configuration, ternary Ni-Cr-Al

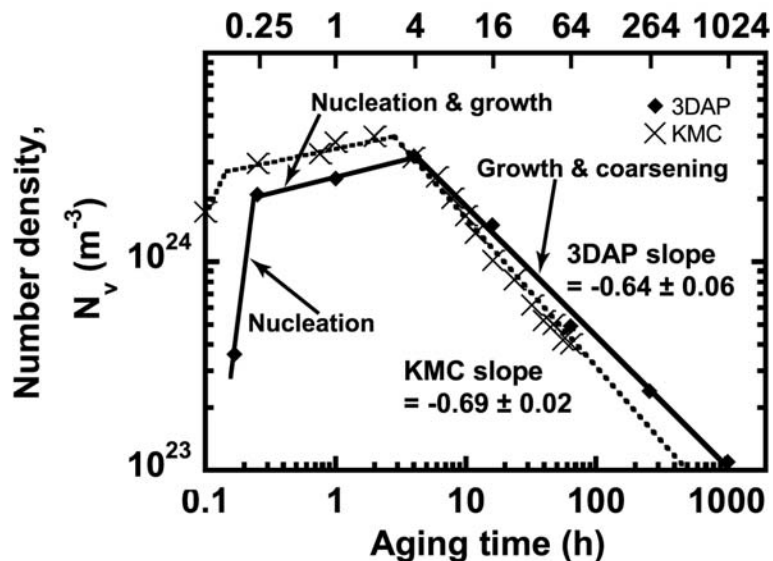


Figure 1: The kinetic Monte Carlo (KMC) simulation results of the temporal evolution of a model Ni-Cr-Al superalloy (Ni-14.8 Cr-5.2 Al at.%) graphed against 3DAP microscopy experimental analysis. The three main stages of precipitate formation — nucleation, growth, and coarsening — are shown. Of particular importance for this study are alloys still in the nucleation stage of precipitate formation.¹

The Effects of Supersaturation on the Nucleation of Precipitates in Nickel-Based Superalloys (*continued*)

superalloys offer excellent high-temperature strength and ductility. This $\gamma+\gamma'$ nanostructure also improves the resistance to applied stress under high temperatures (creep resistance) due to the restricted movement of dislocations,³ forcing them to either climb over the precipitates, loop around by means of the Orowan mechanism,⁴ or simply shear through the precipitate to advance through the lattice if the precipitates are below a critical size. In addition, the native oxides of Cr and Al provide exceptional corrosion and oxidation resistance in Ni-Cr-Al superalloys.⁵ Also in Ni-Cr-Al alloys, the addition of Cr to the binary Ni-Al system helps to reduce the lattice misfit parameter between the γ and γ' phases, thereby impeding the coarsening process of precipitate development.

The origin and nanostructural development of $L1_2$ precipitates in Ni-Cr-Al superalloys can be simplified into three

steps: nucleation, growth, and coarsening (Figure 1). In nickel-based superalloys, both the nucleation and growth stages are short-lived, making them difficult to study. Specifically, this investigation will attempt to focus on the shorter of the two stages, nucleation of precipitates, or embryonic development (sub-critical size nuclei) of precipitates. Nucleation is an important research topic as it is in essence the stage where precipitates are created. Understanding more about this process may aid both the discovery of the most efficient superalloys (based on optimum aging times) and the selection of the best refractory elements.

Background

The potential of nickel-based superalloys was discovered more than 40 years ago when alloy strength was noted to increase anomalously with increasing temperature.⁶ Since then research has concentrated on

enhancing this effect, in this case with Ni-Cr-Al alloys. Among the first superalloys ever developed were the wrought Nimonic 75 and 80 nickel-based superalloys. An important feature of these was the use of Al and Ti to attain age-hardening by the precipitation of γ' phase. The evolution of nickel-based superalloys continued to produce alloys that are still used today, including In-100, 713 C, B-1900, Udimet 500, and Rene 77. These alloys are strengthened predominantly using aluminum, titanium, niobium, and tantalum, which alloy with nickel to form γ' -precipitates.⁵ Superalloys are of great technological importance, having immense potential for high-temperature applications, and three-dimensional atom probe (3DAP) microanalysis has been an excellent means of observing the morphologic differences in nanoscale chemistry for each specific alloy and aging time.

Approach

To best study the nucleation phase of precipitation, three alloys were chosen close to the solvus line of the Ni-Cr-Al phase diagram (Figure 2). Choosing alloys along the solvus line ensures a low supersaturation, which in turn decreases the driving force for nucleation. The main purpose of this study was to select an alloy with a low driving force for precipitate growth. The results from this investigation will be compared with the Ni-14.8 Cr-5.2 Al at.% alloy, and a single alloy will be chosen for a direct study of the nucleation of precipitates.

3DAP Specimen Preparation

A blank of each alloy studied was provided by R. Noebe at the NASA John H. Glenn Research Center. Samples for 3DAP microscopy were prepared from square rods (0.3 mm x 0.3 mm x 10 mm)

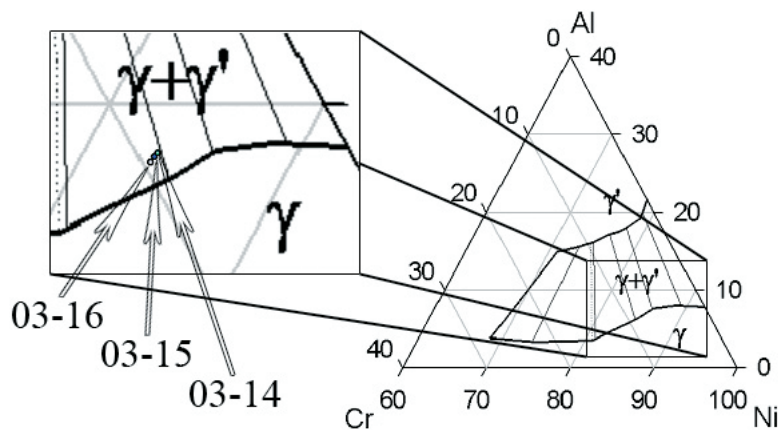


Figure 2: Location of 03-14, 03-15, and 03-16 alloys on the partial Ni-Cr-Al phase diagram at 600° C. The alloys were intentionally chosen close to the $\gamma+\gamma'/\gamma'$ solvus line to obtain a low supersaturation and therefore a low driving force for precipitation.⁷

and were electropolished⁷ in a cuvette using a 10 vol.% perchloric acid in acetic acid solution at 15 V_{dc} at room temperature (Figure 3). Once a smooth cylindrical blank with a diameter of approximately 100 μm was obtained, the samples were further electropolished under a microscope in a platinum loop containing 2 vol.% perchloric acid in 2-butoxyethanol at 9 V_{dc} until a thin (~100 nm radius) neck region was formed. The sample was then electropolished a final time in a cuvette containing 2 vol.% perchloric acid in 2-butoxyethanol at 9 V_{dc} until the neck broke, leaving a tip with a radius of approximately 10–50 nm.

Field Ion Microscopy (FIM)

Before 3DAP microscopy could be performed, FIM was used to align the sample.⁸ In the main chamber of the atom probe, the tip was cooled to 40 K to minimize surface diffusion, and an inert imaging gas (Ne) was introduced until the pressure reached 1.0×10^{-5} torr (gauge pressure). At this point an increasing voltage was applied to the tip until the full crystallographic orientation of the sample was observed due to the field evaporation of the atoms on the surface of the tip. In order to easily calibrate the data that will be collected from a 3DAP microanalysis, the sample must be aligned along the 001 pole, which can be recognized by its fourfold symmetry (Figure 4). The $L1_2$ ordered precipitates along this low index direction ([001]) are desired for the spatial calibration of the three-dimensional reconstruction. Once aligned, 3DAP analysis was performed, and surface atoms were field-evaporated atom by atom and plane by plane due to the electric pulse voltage applied at a fraction of 19 percent¹ of the standing DC imaging voltage and at a frequency of 1.5 kHz.

3DAP Calibration and Analysis

For the data collected from the 3DAP microscope to accurately represent the actual nanostructure, it must first be calibrated. Histograms of the mass-to-charge state (m/z) ratio for the atoms collected were created (Figure 5), and using the ranges of the peaks for H, Al^{2+} , Al^{3+} , Cr^{2+} , and Ni^{2+} in comparison with the accepted values for these ranges, each field-evaporated ion collected during an analysis can be labeled correctly in the three-dimensional reconstruction.

After mass calibration, a three-dimensional reconstruction of the ions collected during a trial is created using ADAM 1.5b13⁹, a Mac OS–based program written and developed by members of Professor Seidman's group specifically for visualization analyses and visualization of data obtained through 3DAP microanalysis. As with the mass spectra, the length, width, and depth of the three-dimensional representation have to be rescaled as well. The depth (z-axis) scale can be fine-tuned by measuring the relative spacing of the Al planes in the γ' precipitates from the three-dimensional image, comparing it to the known accepted value, and adjusting accordingly. After the z-axis is calibrated, the x-y plane can be effectively rescaled by contrasting the measured density with the accepted theoretical density for that specific alloy composition. Here, the expected density is 86 atoms/ nm^3 , but the atom probe has a detection efficiency of 60 percent, making the desired density 52 atoms/ nm^3 . From these three-dimensional reconstructions, the presence of any γ' precipitates within the γ matrix can be detected.

Transmission Electron Microscope (TEM)

TEM samples were prepared by mechanically polishing a 10 mm x 10 mm sheet

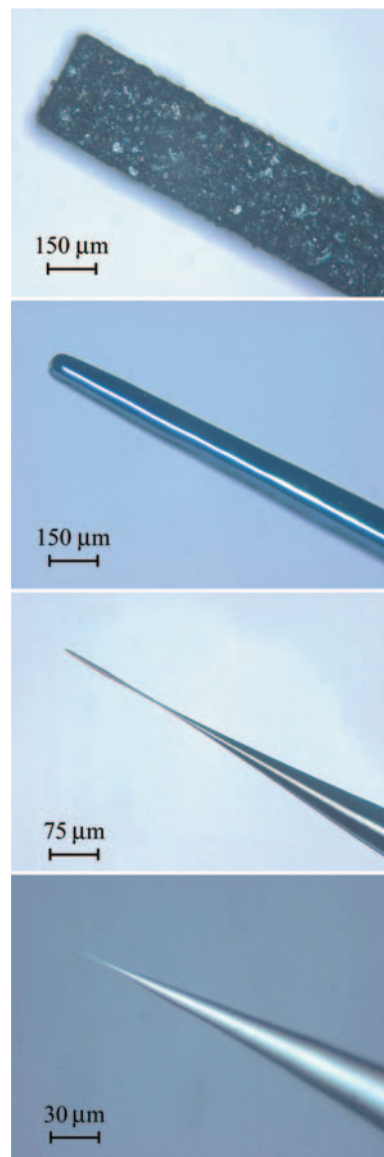


Figure 3: Optical micrographs of the stages of tip preparation for 3DAP analysis. The apex of the final tip is < 50 nm. Nanoscopically sharp tips are required for FIM and 3DAP microanalysis.

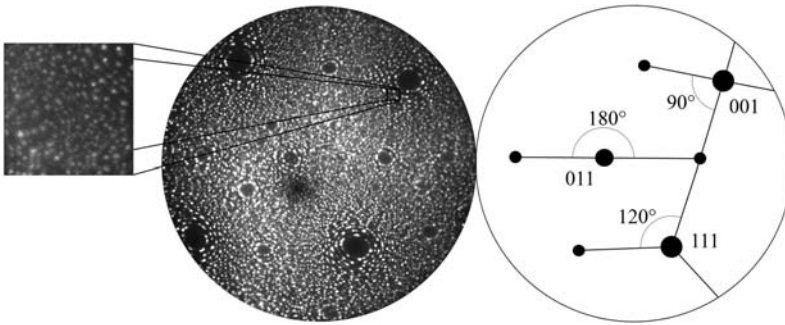


Figure 4: FIM image of alloy 03-15 cooled to 40 K in a Ne environment at 1×10^{-9} torr, revealing the crystallographic orientation of the tip. Each spot represents a single atom. 3DAP microanalysis was carried out along 001 pole (inset), which can be easily recognized by its four-point symmetry. Also visible are the 011 and 111 poles with their twofold and threefold symmetries, respectively.

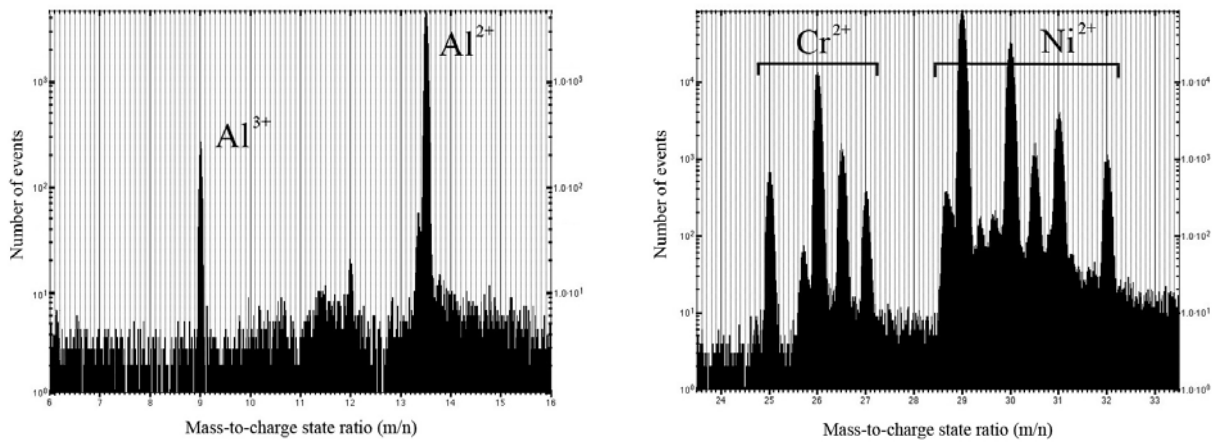


Figure 5: Mass spectra histograms showing the mass-to-charge state ratios of ions collected during 3DAP analysis of alloy 03-15. Each peak in the histogram represents an isotope of its corresponding element. The width of the peaks represent the range of ions for each element's charge state and are used to calibrate the 3DAP three-dimensional reconstructions.

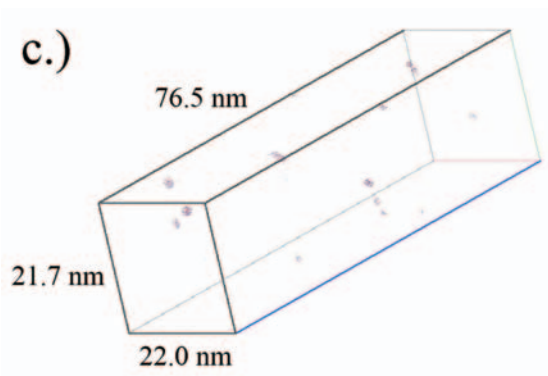
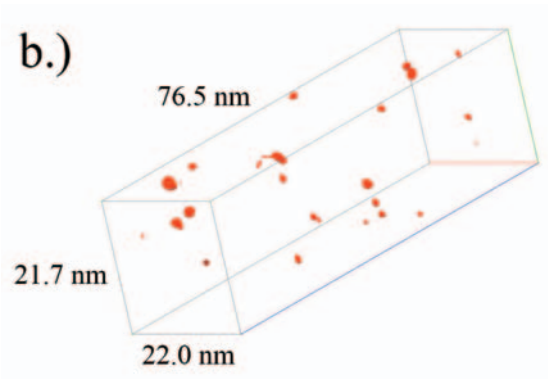
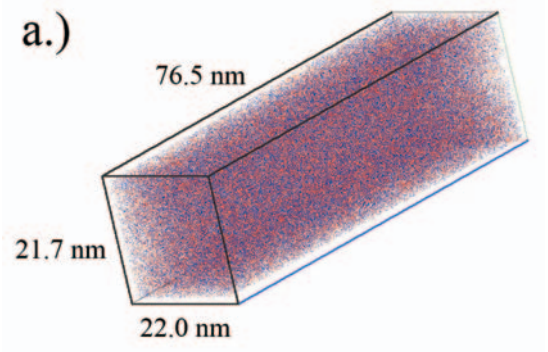


Figure 6: Three-dimensional reconstructions of alloy 03-15, showing atoms of chromium (blue) and aluminum (red); nickel atoms have been omitted for clarity. 6a is overall composition, 6b is of isoconcentration surfaces, which delineate the γ -matrix and the γ' -precipitates, and 6c is of atoms contained within ordered γ' -precipitates.

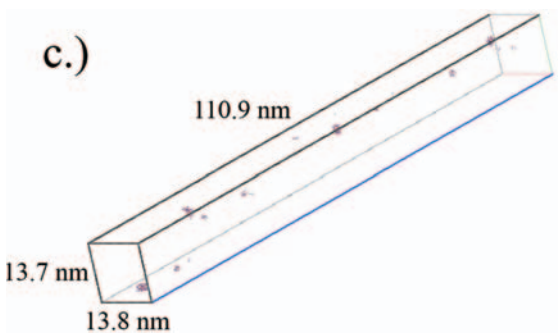
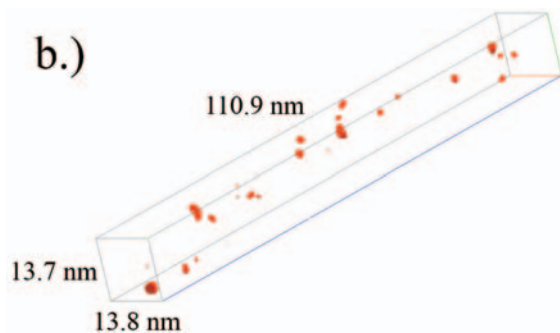
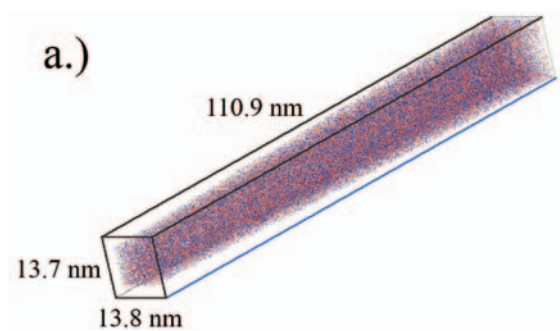


Figure 7: Three-dimensional reconstructions of alloy 03-16, showing atoms of chromium (blue) and aluminum (red); nickel atoms have been omitted for clarity. 7a is overall composition, 7b is of isoconcentration surfaces, which delineate the γ -matrix and the γ' -precipitates, and 7c is of atoms contained within ordered γ' -precipitates.

The Effects of Supersaturation on the Nucleation of Precipitates in Nickel-Based Superalloys (*continued*)

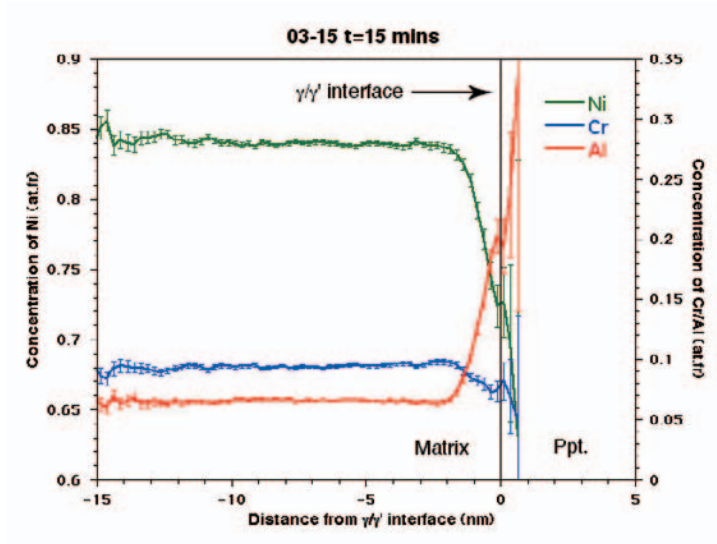


Figure 8: Proximity histogram (proxigram) showing the concentrations of Ni, Cr, and Al as a function of distance (nm) near the γ/γ' interface for alloy 03-15. As we move from the γ -matrix (predominantly nickel) to the γ' -precipitates (nominal Ni_3Al composition), the concentrations of nickel and chromium decrease and, inversely, the concentration of aluminum increases.

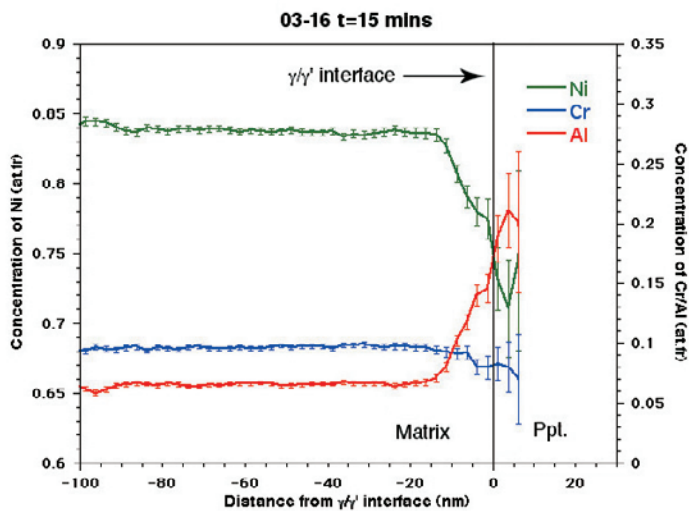


Figure 9: Proximity histogram (proxigram) showing the concentrations of Ni, Cr, and Al as a function of distance (nm) near the γ/γ' interface for alloy 03-16. As we move from the γ -matrix (predominantly nickel) to the γ' -precipitates (nominal Ni_3Al composition), the concentrations of nickel and chromium decrease and, inversely, the concentration of aluminum increases.

of each alloy to a thickness of about 100 μm . From the polished sample, discs with a diameter of approximately 3 mm were cut. Each disk was then electropolished with a twin-jet Streuers TenuPol-5 using a 12 vol.% perchloric acid in methanol solution at -30°C and 13 V_{dc} , until a perforation was formed in the center of a disk, with a thickness of about 50 nm near the edge of the hole. The selected-area diffraction patterns for each of the samples were then analyzed for crystal structure and the presence and confirmation of ordered precipitates.

Results and Discussion

3DAP Three-Dimensional Reconstructions

The three-dimensional atom-by-atom reconstructions for 03-15 and 03-16 aged for 0.25 hours at 600°C were then done using ADAM. Chromium atoms are shown in blue, and aluminum atoms in red; for the sake of clarity, nickel is omitted from the overall reconstructions (Figures 6a, 7a). Due to the short aging time (0.25 hours), the γ' -precipitates in each of these alloys are on a small sub-nanometer scale and are most likely either

embryos (sub-critical size nuclei), or nuclei. At a threshold value of 11 at.% Al for alloy 03-15, the isoconcentration surface, which delineates the γ/γ' interface, can be distinguished (Figure 6b). For the case of 03-16, no precipitates were present for a threshold value of 11 at.% Al, so a lower threshold (9 at.% Al) was necessary to visualize the formation of nuclei and/or embryos (Figure 7b). Also displayed are the resident Ni, Cr, and Al atoms inside each precipitate (Figures 6c, 7c).

To better understand the interface between the γ and γ' phases, proximity histograms¹⁰ (proxigrams) were created using ADAM (Figures 8, 9). These proxigrams show the transition from γ -matrix to γ' -precipitates by analyzing all the precipitates in the volume simultaneously and determining the exact concentrations of each element as a function of distance from the γ/γ' interfaces. Understanding these diagrams helps to describe the precise elemental composition of an alloy's γ' -precipitates on a nanoscale level.

Using the data generated from the three-dimensional reconstructions and the proxigrams, the concentrations of both

the matrix and the precipitates are calculated (Table 1). The atoms that are considered to be a part of the γ' precipitates are those located within the isoconcentration surfaces with at least 10 atoms per precipitate. The detected precipitates with less than 10 atoms per precipitate are omitted, since they are falsely identified by the ADAM program as precipitates due to aberrations in the x-y plane. Similarly, those considered to be a part of the γ -matrix are those that are not contained within the isoconcentration surfaces.

From the refined data, the mean radius ($\langle R \rangle$), number density (N_v), and volume fraction (V_f) of the precipitates for each alloy were measured (Table 2). The radii of individual precipitates were determined by ADAM, which established the center-of-mass of each precipitate, calculated the average radius, and averaged that value for every precipitate. The number density was calculated by counting the total number of precipitates in the three-dimensional reconstruction and dividing that by the total analysis volume. Finally, the volume fraction was measured by

Table 1: Atomic percent of Ni, Cr, and Al in both the γ -matrix and γ' -precipitates for alloys 00-1, 03-14, 03-15, and 03-16 aged at 600°C for 0.25 hours.

Alloy	Matrix (at.%)			Precipitate (at.%)		
	Ni	Cr	Al	Ni	Cr	Al
Ni-14.8 Cr-5.2 Al at.% (00-1)	80.560 \pm 0.060	14.270 \pm 0.055	5.170 \pm 0.035	73.120 \pm 0.93	9.410 \pm 0.60	17.470 \pm 0.80
Ni-9.0 Cr-7.0 Al at.% (03-14)	83.964 \pm 0.032	9.046 \pm 0.025	6.990 \pm 0.022	74.564 \pm 2.57	4.878 \pm 1.27	20.557 \pm 2.39
Ni-9.25 Cr-6.75 Al at.% (03-15)	83.909 \pm 0.027	9.428 \pm 0.022	6.662 \pm 0.018	71.452 \pm 1.82	7.993 \pm 1.10	20.555 \pm 1.63
Ni-9.5 Cr-6.5 Al at.% (03-16)	83.760 \pm 0.039	9.634 \pm 0.031	6.602 \pm 0.026	72.612 \pm 1.51	8.400 \pm 0.94	18.987 \pm 1.33

The Effects of Supersaturation on the Nucleation of Precipitates in Nickel-Based Superalloys (*continued*)

Table 2: Average precipitate radius (<R>), number density (N_v), and measured and calculated volume fractions (V_f) of the γ' -precipitates for 00-1, 03-14, 03-15, and 03-16 alloys aged at 600° C for 0.25 hours. Also calculated was the percent difference between the measured and calculated values for volume fraction.

Alloy	<R> (nm)	N_v (m^{-3})	V_f (%) (measured)	V_f (%) (calculated)	V_f Percent Difference
Ni-14.8 Cr-5.2 Al at.% (00-1)	0.75	2.1×10^{24}	0.55	0.37	32.7
Ni-9.0 Cr-7.0 Al at.% (03-14)	0.605	1.99×10^{23}	0.022	0.018	18.2
Ni-9.25 Cr-6.75 Al at.% (03-15)	0.527	3.56×10^{23}	0.034	0.022	35.3
Ni-9.5 Cr-6.5 Al at.% (03-16)	0.511	3.56×10^{23}	0.098	0.020	79.6

dividing the total number of atoms within the precipitates by the total number of overall atoms that were collected during a 3DAP microscopy analysis. The volume fraction was also calculated using the following formula, where the precipitates are assumed to be spherical:

$$\frac{4}{3}\pi \langle R \rangle^3 N_v = V_f$$

The values for each method of determining the volume fraction were compared and the percent difference was calculated.

The results for the latter three alloys are more favorable for further study of the nucleation of precipitates, since the results for mean precipitate radius, number density, and volume fraction are smaller, indicating that the driving force for precipitation is lower. This is expected, as these alloys lie closer to the $\gamma/\gamma+\gamma'$ solvus line, implying that they have lower supersaturations, which governs the driving force for nucleation. Of the three alloys analyzed in this study, 03-16 seems to be the most promising for studying the nucleation of $L1_2$ ordered precipitates, because the mean radius of the precipitates

is the lowest of the three alloys. Also, these numbers are based on the 9 at.% Al threshold value entered when ADAM explored the data for precipitates, whereas the other two are based on an 11 at.% Al threshold value. This signifies that the precipitates for alloy 03-16 are less developed than the others, as an 11 percent threshold value for 03-16 produced no observable precipitates, meaning that they have not yet developed into nuclei and perhaps are still in the embryonic stage of precipitate formation. This is promising for an effective study of nucleation in Ni-Cr-Al superalloys, and 03-16 is the best candidate for further study.

TEM Analysis

The TEM micrograph gave a clear picture of what could be recognized as the diffraction pattern of a 001 pole. To confirm that the pattern is due to Ni planes, the distance between distinct points on the micrograph (R), the wavelength of the incident beam (λ), and the camera length (L) were entered into the following formula, and the planar spacing was determined and compared with the actual value:

$$2Rd = \lambda L$$

$$2(.014)d = 2.73 \times 10^{-12}(1)$$

$$d = .359 \times 10^{-9}$$

It can be concluded that, compared with the actual value of 0.356×10^{-9} , the pattern is resultant of Ni planes from the sample. Also visible in the diffraction patterns produced by the TEM analysis are superlattice reflections (Figure 10), which only appear when there are $L1_2$ ordered γ' -precipitates present.

Conclusions

Using 3DAP microscopy, the nanostructure and nanoscale chemistry of γ' -precipitates in a total of three nickel-based superalloys were observed. Of the alloys analyzed, Ni-9.5 Cr-6.5 Al at.% (03-16) proved to have the most favorable attributes. Due to its lower driving force for nucleation, as indicated by its lower <R> value at a lower threshold value for defining what is even considered to be a precipitate, 03-16 can be classified as the best alloy for future in-depth study of the nucleation of $L1_2$ -type Ni_3Al ordered γ' -precipitates. Using TEM analysis, the

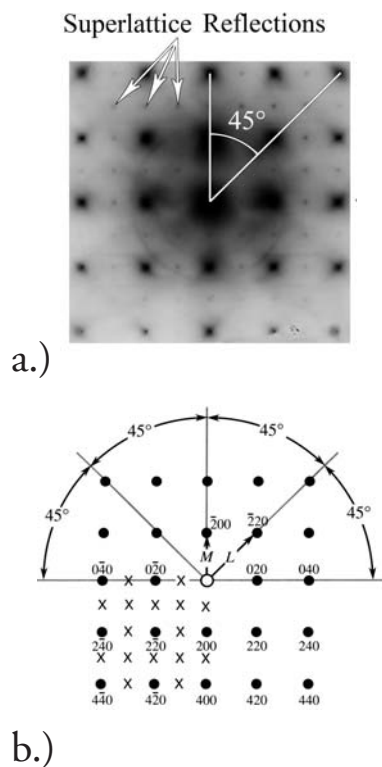


Figure 10: (a) TEM micrograph showing the diffraction pattern of the 001 pole in alloy 03-15. The pattern shows correspondence with the diffraction pattern produced by the 001 pole in a predominantly nickel γ -matrix, shown in (b). Also visible are superlattice reflections, which only appear in the diffraction pattern when $L1_2$ ordered γ' -precipitates are present.

conclusion that the precipitates viewed in the three-dimensional reconstructions were in fact $L1_2$ ordered Ni_3Al γ' -precipitates could be established due to the appearance of superlattice reflections in the diffraction pattern for the 001 pole.

To get a better view of how nucleation progresses for this alloy, future research will comprise 3DAP analysis of a series of aging times of the said 03-16 alloy, including an unaged sample. A comparison of the data obtained from these supplementary aging times will help shed light on the poorly understood process of nucleation of precipitates in nickel-based superalloys.

References

- (1) Yoon, K. E. PhD thesis, Northwestern University, Evanston, IL, 2004.
- (2) Wahll, M. J.; Maykuth, D. J.; Hucek, H. J. *Handbook of Superalloys*; Batelle Press: Columbus, OH, 1979, pp 1–2.
- (3) Tottle, C. R. *An Encyclopaedia of Metallurgy and Materials*; Macdonald & Evans: Plymouth, Great Britain, 1984, pp 75–76.
- (4) Hull, D.; Bacon D. J. *Introduction to Dislocations*, 3rd ed.; Butterworth-Heinemann: Oxford, Great Britain, 1984, pp 16, 151–152.
- (5) Sims, C. T.; Hagel, W. C. *The Superalloys*; John Wiley & Sons: New York, 1972, p 3.
- (6) Westbrook, J. H. *Trans. AIME* **1957**, *209*, 898.
- (7) Sudbrack, C. K.; Yoon, K. E.; Mao, Z., et al. *Temporal Evolution of Nanostructures in a Model Nickel-Base Superalloy: Experiments and Simulations* In *Electron Microscopy: Its Role in Materials Science*; Weertman, J. R.; Fine, M.; Faber, K., et al. TMS: Warrendale, PA, 2003.
- (8) Miller, M. K.; Smith, G. D. W. *Atom Probe Microanalysis: Principles and Applications to Materials Problems*. Materials Research Society: Pittsburgh, PA, 1989, pp 2–7, 43–50.
- (9) Hellman, O. C.; Vandenbroucke, J.; Blatz du Rivage, J., et al. *Mat. Sci. Eng. A* **2002**, *327*, 29–33.
- (10) Hellman, O. C.; Vandenbroucke, J. A.; Rusing, J., et al. *Microsc. Microanal.* **2000**, *6*, 437–444.
- (11) Williams, D. B.; Carter, C. B. *Transmission Electron Microscopy: Diffraction*; Plenum Publishing Corporation: New York, 1996, p 282.